Energy-Based Solution Method for the Global Behavior of Diaphragms under Pneumatic and Electrostatic Pressure

Olivier Français and Isabelle Dufour

Laboratoire d'Electricité Signaux et Robotique (LESiR) - URA CNRS 1375 -
Ecole Normale Supérieure de Cachan, 61 avenue du président Wilson, 94235 Cachan Cedex, France
tel: 33-1-47-40-27-11 fax: 33-1-47-40-27-08 e-mail: francais@lesir.ens-cahan.fr

ABSTRACT

In this paper, an approximate analytical solution is presented for the diaphragm's deflection based on energy minimization, through the use of a polynomial solution technique. Thanks to this method, we obtain not only the center deflection, but also the entire position under pneumatic pressure, thereby making it possible to compute the diaphragm's deflected volume. Regarding the geometrical and physical parameters, three cases can be distinguished. with the diaphragm: acting as a pure plate, acting as a pure membrane, or exhibiting the effects of both the elastic rigidity and the initial internal stress. For these three cases, a standardization of the diaphragm's behavior enables obtaining an abacus that can then be used for any geometrical or physical parameter. In order to validate this approach, some comparisons with other methods are performed. This energy-based approach has been extended to electrostatic actuation and yields more general results than do other more classical methods (i.e., the spring model). Lastly, a behavioral comparison of both the membrane and plate cases is presented for a conformable mirror with electrostatic actuation.

keywords: diaphragm, pneumatic, electrostatic, deflection

INTRODUCTION

In this paper, we consider a built-in diaphragm (Fig. 1) characterized by its thickness h, its width a, its length b, its elastic flexural rigidity $D_0 = E/12(1-\nu^2)$, where E is the Young's modulus and ν the Poisson's ratio, and its initial internal stress T_0. The deflection under pressure p(x,y) has been denoted by w(x,y). The study presented below is limited to small deflections ($w < h$).

The classical law governing the diaphragm's behavior under such assumptions and notations is [1]:

$$D_0 h^3 \Delta\Delta w(x,y) - T_0 h \Delta w(x,y) = p(x,y) \qquad (1)$$

where: $\Delta = \frac{\partial^2}{\partial x^2} + \frac{\partial^2}{\partial y^2}$.

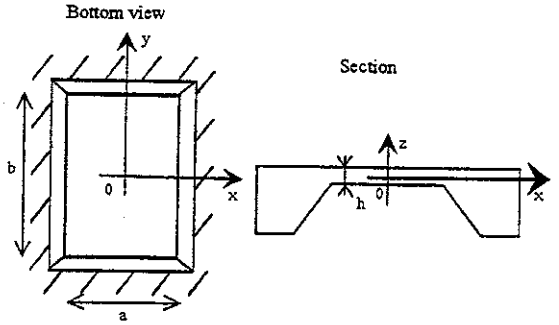

Figure 1: Geometry of the diaphragm

There is no simple analytical solution to equation (1). The solution can thus be obtained with FEM simulation or approximate solution methods. In order to derive a parametric solution, we have opted for the approximate solution method based on energy minimization.

ENERGY MINIMIZATION

The deflection w(x,y) of a diaphragm under pressure p(x,y) corresponds to the diaphragm position that has the minimum total energy. We have chosen to approximate this deflection by a linear combination of polynomial functions f_i:

$$w(x,y) = \sum_{i=1}^{n} a_i f_i(x,y) \qquad (2)$$

Let U_{tot} represent the total energy of the diaphragm; the deflection is then obtained with the n coefficients a_i, solutions to the n equations:

$$\frac{\partial U_{tot}}{\partial a_i} = 0 \qquad (3)$$

Energy Calculation

The total energy of the diaphragm is composed of two terms [2]:

- the potential energy due to pressure acting on the diaphragm:

$$U_{ext} = \int_{-b/2}^{b/2} \int_{-a/2}^{a/2} \left(\int_0^w p(x,y)dw \right) dxdy \qquad (4)$$

- and the potential internal energy due to both the

elastic flexural rigidity D_0 and the initial internal stress T_0:

$$U_{int} = U_{D_0} + U_{T_0} \quad (5)$$

with:

$$U_{D_0} = \frac{1}{2}\int_{-b/2}^{b/2}\int_{-a/2}^{a/2} D_0 h^3 \left(\Delta\Delta w(x,y)\right) w(x,y)\, dxdy \quad (6)$$

and:

$$U_{T_0} = -\frac{1}{2}\int_{-b/2}^{b/2}\int_{-a/2}^{a/2} T_0 h \left(\Delta w(x,y)\right) w(x,y)\, dxdy \quad (7)$$

Therefore, the total energy can be expressed as:

$$U_{tot} = U_{ext} + U_{int} = U_{ext} + U_{D_0} + U_{T_0} \quad (8)$$

Coefficient Calculation

Given the expression for the total energy, the n equations (3) can be combined into matrix form, as follows:

$$\left[\ \frac{dU_{int}}{da_i}\ \right]\cdot\left[a_i\right] = -\left[\frac{dU_{ext}}{da_i}\right] \quad (9)$$

where:

- dU_{int}/da_i is a (nxn) matrix that contains, for each row 'i' - column 'j' pair, the second partial derivative of the U_{int} energy with respect to the 'ith' and 'jth' coefficients. It should be noted that this matrix is not dependent upon the type of excitation. Instead, it depends solely upon the approximate functions f_i.
- a_i is a (nx1) vector that contains the n coefficients a_i.
- dU_{ext}/da_i is a (nx1) vector that contains the derivatives of U_{ext} with respect to each of the coefficients a_i.

The coefficients a_i can then be derived as follows:

$$\left[a_i\right] = \left[\ \frac{dU_{int}}{da_i}\ \right]^{-1}\cdot\left[\frac{dU_{ext}}{da_i}\right] \quad (10)$$

In this equation, the two matrices are dependent upon the approximate functions f_i. In the following section, we will show that the number n and the choice of the n functions both serve to determine the accuracy of the results.

Choice of Polynomial Functions

In order to avoid the constraints of the diaphragm's dimensions, the following variable substitution is introduced: $X = 2x/a$; $Y = 2y/b$, with the origin being located at the center of the diaphragm: $X \in [-1,1]$ and $Y \in [-1,1]$. The expression of the deflection can then be written with the new variables:

$$W(X,Y) = \sum_{i=1}^{n} A_i F_i(X,Y) \quad (11)$$

where:

$$W(X,Y) = w(aX/2, bY/2)$$

and: $F_i(X,Y) = f_i(aX/2, bY/2)$

The polynomial functions F_i must be in agreement with the built-in diaphragm's boundary conditions:

$$F_i(\pm 1, Y) = F_i(X, \pm 1) = 0 \text{ and } \frac{\partial F_i(\pm 1, Y)}{\partial X} = \frac{\partial F_i(X, \pm 1)}{\partial Y} = 0$$

The function F_i has therefore been chosen with the term $\left(1-X^2\right)^2\left(1-Y^2\right)^2$ as a factor. Moreover, since only symmetrical actuation is being considered, the approximate functions must be even. The simplest functions corresponding to these criteria are [3]:

$$(1-X^2)^2 (1-Y^2)^2 X^j Y^k \quad (12)$$

with j and k being even numbers.

If the numbers j and k were to increase, the polynomial functions would get shifted towards the edges of the diaphragm. Thus, from Fig. 2 (with all of the function maxima being taken as equal to 1), we can observe that it is not necessary to use many functions of this type, in that the functions corresponding to high polynomial orders will be of little significance in the deflection's estimation.

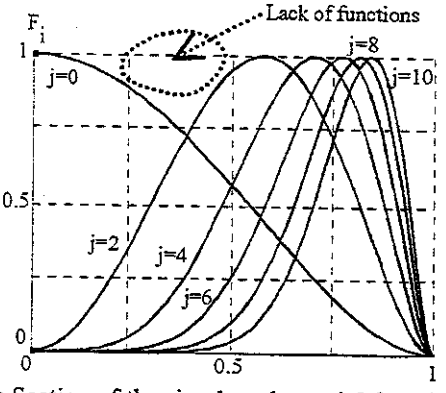

Figure 2: Section of the simple polynomial functions: Y=0

In order to compensate for the lack of functions in the intermediate zone between the edge and the center, we propose employing other polynomial functions:

$$(1-X^2)^{2+nl}(1-Y^2)^{2+nm} X^{2l} Y^{2m} \quad (13)$$

with: $(l, m) \in \{(0,1), (1,0), (1,1)\}$ and n being an even number.

For the following simulations, we have considered 34 F_i functions:

- 25 of the first type (equation (12)), with $j \in \{0;2;4;6;8\}$ and $k \in \{0;2;4;6;8\}$; and
- 9 of the second type (equation (13)), with $n \in \{2;4;6\}$ and $(l,m) \in \{(0,1),(1,0),(1,1)\}$.

In order to visualize the area corresponding to the localization of the functions, the contour of the various F_i functions has been plotted in the [X,Y] plane, with the maxima taken as equal to 1 for each function and with a contour value equal to 0.98 (see Fig. 3). The gray areas correspond to values of less than 0.98 and the white areas to values of greater than 0.98. The first type of functions have been indicated by solid lines and the second type of functions by dashed lines.

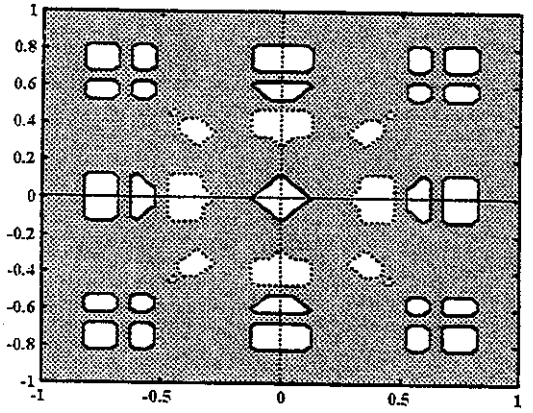

Figure 3: Contour of the F_i functions (limit = 0.98)

Fig. 3 demonstrates the advantage of using functions of the second type (in the intermediate zone) instead of a greater number of functions of the first type (placed along the edges).

PNEUMATIC ACTUATION

In the previous section, a methodology for solving equation (1) was presented. The result with respect to the deflection under pneumatic pressure $(p(x,y) = constant = P_0)$ depends on the diaphragm's geometrical characteristics (h, a and b) as well as on its physical parameters (D_0 and T_0). In this section, the case of the plate (the opposite force due to T_0 is negligible) and the case of the membrane (the opposite force due to D_0 is negligible) are to be examined first. Once these two cases have been taken into consideration, the deflection can then be standardized. Afterwards, we will show that, for some determinate diaphragm configurations, these two simpler cases cannot actually be applied. For such configurations, another standardization procedure has thereby been proposed.

Plate Behavior

In this case, equation (1) becomes:

$$D_0 h^3 \Delta\Delta w(x,y) = P_0 \qquad (14)$$

This equation is equivalent to:

$$r^2 \frac{\partial^4 N_D}{\partial X^4} + 2\frac{\partial^4 N_D}{\partial X^2 \partial Y^2} + \frac{1}{r^2}\frac{\partial^4 N_D}{\partial Y^4} = 1 \qquad (15)$$

with:

- $N_D(X,Y) = W(X,Y) / C_D$
- $C_D = \dfrac{P_0 S^2}{16 D_0 h^3}$
- $r = b/a$

Thus, for a given rectangularity (r being fixed), the solution to equation (15) with the method presented in this article's "energy minimization" section is sufficient in order to determine the deflection for each geometrical and physical parameter. The product of the solution $N_D(X,Y)$ to equation (15) and the value of C_D is in fact the deflection W(X,Y).

In Fig. 4, the solution $N_D(0,0)$ to equation (15) has been plotted versus the value of the rectangularity r. Moreover, we have plotted in the same figure some of the results published by other authors [4] as well as some FEM simulations performed with the software ANSYS. A very high level of agreement has been observed between our method's results and those based on other methods. This encouraging result serves both to validate the solution method presented herein and to apply it to a more complex case: electrostatic actuation.

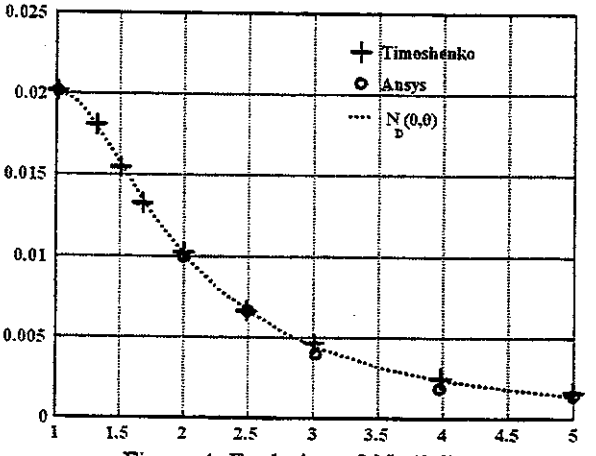

Figure 4: Evolution of $N_D(0,0)$ versus r

Membrane Behavior

In this case, equation (1) becomes:

$$-T_0 h \Delta w(x,y) = P_0 \qquad (16)$$

The same standardization as that employed in the

plate case can be performed for the membrane; equation (16) is then equivalent to:

$$r\frac{\partial^2 N_T}{\partial X^2}+\frac{1}{r}\frac{\partial^2 N_T}{\partial Y^2}=-1 \qquad (17)$$

with:

- $N_T(X,Y) = W(X,Y) / C_T$
- $C_T = \dfrac{P_0 S}{4 T_0 h}$
- $r = b / a$

Thus, like for the plate case, the solution to equation (17) by the method presented in the "energy minimization" section and the calculation of the C_T value are sufficient in determining the total deflection of the membrane. The standardized result for the center deflection, $N_T(0,0)$, has been presented in Fig. 5.

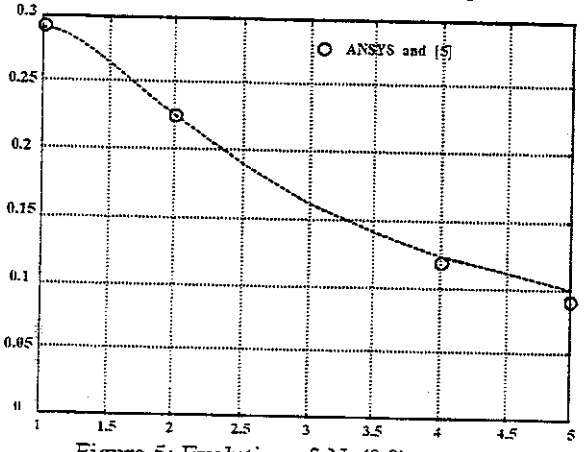

Figure 5: Evolution of $N_T(0,0)$ versus r

It is obvious that in this case, the solution method presented herein is in agreement with other results [5]; hence, this solution principle can indeed be applied to the electrostatic case.

General Case

As for the two previous cases, in order to obtain a standardized result, equation (1) can be written as follows:

$$\Delta\Delta N_{C_{DT}}(X,Y)-\frac{C_D}{C_T}\Delta N_{C_{DT}}(X,Y)=1 \qquad (18)$$

with:

- $N_{C_{DT}}(X,Y) = W(X,Y) / C_D$

In Fig. 6, the result obtained in the square-shaped diaphragm case has been presented for the center point. As opposed to the two simplified cases (plate and membrane), in the general case, the solution depends upon both the rectangularity r and the parameter C_D/C_T.

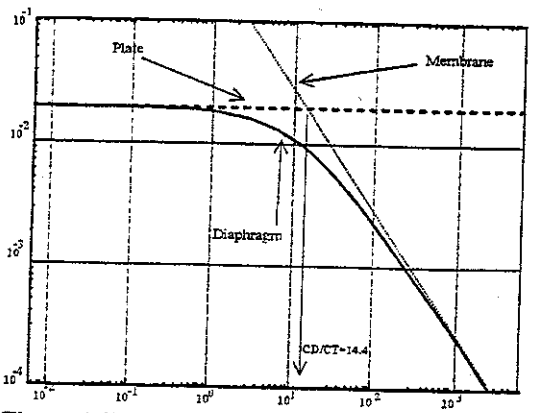

Figure 6: Evolution of $N_{C_{DT}}(0,0)$ versus C_D/C_T

Fig. 6 demonstrates that for some ranges of C_D/C_T, the diaphragm can be considered either as a plate or as a membrane. In the following section, we will examine whether the general case (over the entire C_D/C_T range) can be deduced from the two simplified cases (plate and membrane).

Determination of the simplest solution for each case

It has already been observed that the deflection under pneumatic actuation can be easily solved and standardized into two limit cases (plate and membrane). Next, we will determine under which conditions a diaphragm can be considered as either a plate or a membrane.

In the two limit cases, the deflection of each point (X,Y) can be written as the displacement of a spring with a stiffness K(X,Y), such that:

$$W(X,Y) = P_0/K(X,Y) \qquad (19)$$

with $K(X,Y) = K_D(X,Y) = \dfrac{1}{C_D N_D(X,Y)}$ in the plate case,

and $K(X,Y) = K_T(X,Y) = \dfrac{1}{C_T N_T(X,Y)}$ in the membrane case.

As an initial consideration, if we were to assume that no coupling occurs between the flexural rigidity and the internal stress during deflection, the general case could then be modeled by two parallel springs (K_D and K_T) (see Fig. 7).

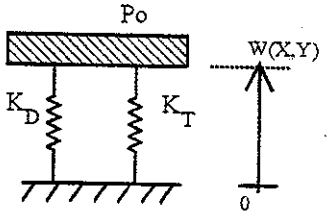

Figure 7: Modeling of both the elastic flexural rigidity D_0 and the initial internal stress T_0

The deflection expression would then become:

$$W(X,Y) = \frac{P_0}{K_T + K_D} = \frac{C_D N_D(X,Y) C_T N_T(X,Y)}{C_D N_D(X,Y) + C_T N_T(X,Y)} \quad (20)$$

If $K_D >> K_T$, the diaphragm can thus be considered as a plate: $W(X,Y) = C_D N_D(X,Y)$. If $K_T >> K_D$, the diaphragm can be considered as a membrane: $W(X,Y) = C_T N_T(X,Y)$. And if $K_T \cong K_D$, the expression in equation (20) must be used.

In Fig. 8, we have plotted the relative error encountered for the center deflection as obtained in the three cases (plate, membrane and two parallel springs) with respect to the general solution to equation (1). Fig. 8 corresponds to a square diaphragm (r = 1).

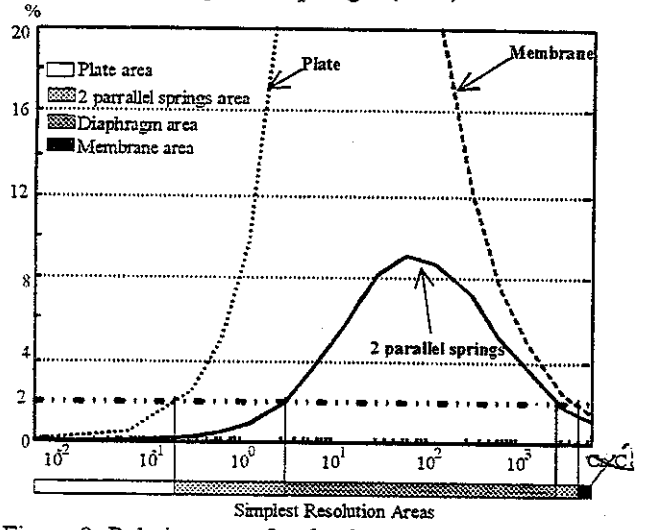

Figure 8: Relative error for the three different case-specific solutions with respect to the general solution versus C_D/C_T for a square diaphragm

Once the limits of an acceptable error have been set (e.g., at 2%), Fig. 8 then enables determining the individual areas (depending on the value of C_D/C_T) where the plate, membrane, two parallel springs or general solution must be applied.

ELECTROSTATIC ACTUATION

In this case, the pressure acting on the diaphragm is not constant, but rather depends on the deflection. An electrode is placed in front of the diaphragm at a distance e, and a voltage U is applied between the diaphragm and the electrode. An electrostatic pressure $P_e(X,Y)$ is then created:

$$P_e(X,Y) = \frac{P_0}{(1 - W(X,Y)/e)^2} \quad (21)$$

with: $P_0 = \frac{\varepsilon U^2}{2e^2}$, and ε is the permeability of the space between the electrode and the diaphragm.

In this section, we will focus our presentation on a square plate. This particular study approach can also be applied to a membrane or a diaphragm.

In this case, equation (1) is equivalent to:

$$\Delta\Delta N_e(X,Y) = \frac{C'}{(1 - N_e(X,Y))^2} \quad (22)$$

with:

- $N_e(X,Y) = W(X,Y)/e$
- $C' = \frac{P_0 S^2}{16 D_0 h^3 e}$

For a fixed value of C' therefore, only one solution for N_e actually exists. Once $N_e(X,Y)$ has been identified as a function of C', deducing the value of W(X,Y) for all plate characteristics is thus made possible:

$$W(X,Y) = eN_e(X,Y)\big|_{C'} \quad (23)$$

In terms of pneumatic actuation, the deflection can be deduced from the abacus. In this case however, for a given rectangularity (r being fixed), simulations with several C' values must be run. C' lies between 0 and the value corresponding to the plate center's pull-in.

To obtain the N_e evolution with respect to C', the energy minimization method has once again been used. Furthermore, we have developed an iterative calculation procedure to determine the coefficients a_i. At each increment of the calculation, the new position is integrated into the pressure in order to converge towards the solution.

Fig. 9 presents the standardization of the center deflection, $N_e(0,0)$. Other authors [6] have classically presented the limit prior to the pull-in effect as a displacement corresponding to one-third of the e value. In this instance, using the energy-based method, we have obtained a limit displacement that corresponds to a larger value than the displacement for which C' is equal to 11.

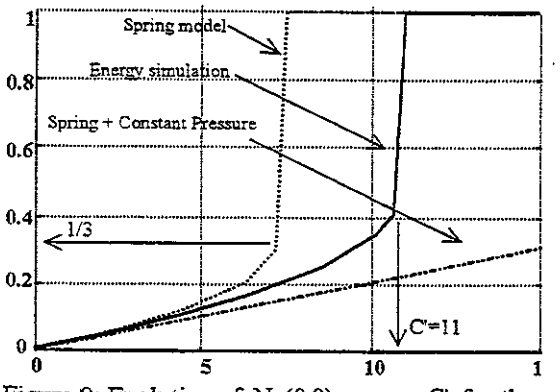

Figure 9: Evolution of $N_e(0,0)$ versus C' for three different models

A comparison with two more classical methods has been performed in Fig. 9: one method considers the pressure to be constant, while the other models the membrane by using independent constant springs [7]. It appears that for very small deflections, the pressure can indeed be considered as a constant. For larger deflections, the model based on independent springs is appropriate in order to understand and estimate both the pull-in and pull-out effects. However, for high voltages, the pull-in effect changes the system's behavior, and, at this point, the spring model is no longer sufficient in producing an accurate simulation (in terms of both the capacity estimation and the estimation of deflected volume).

The same curve can be derived for the volume corresponding to the membrane's deflection. In this case, we have to simulate for a higher value of C' than the value used for $C'_{pull-in}$. This simulation also proves more complicated in that the contact between one electrode and another electrode in the presence of both an insulator and a contact force must be integrated.

USE OF RESULTS

In order to compare the plate and membrane behavioral patterns, a simulation of a conformable mirror with electrostatic actuation has been carried out. It has been observed that a diaphragm can be considered, under certain conditions, as either a plate or a membrane. Hence, it may prove interesting to compare the deflection obtained in these two cases as a means of determining the material's influence.

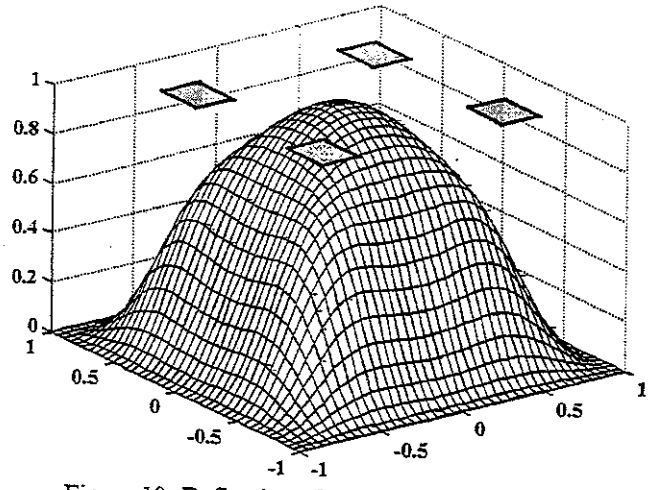

Figure 10: Deflection of a plate with 4 electrodes

We can note the different behavioral patterns of the diaphragm in the two limit cases. In order to generate a complicated deflection, it is advisable to use a membrane rather than a plate. A membrane actually reflects the structure of the electrode to a greater extent than does a plate, which yields a smoother deflection.

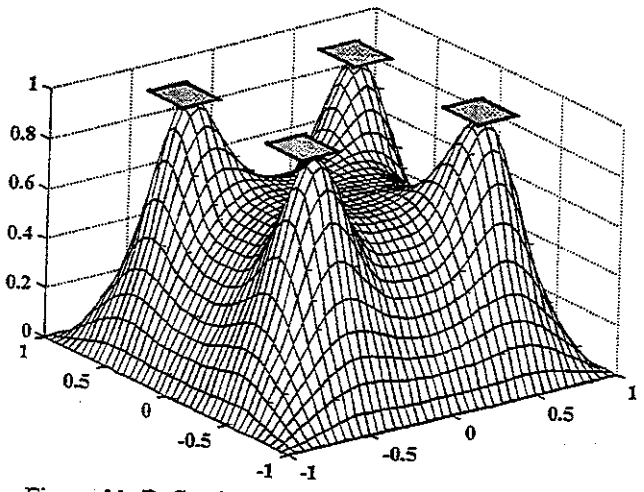

Figure 11: Deflection of a membrane with 4 electrodes

CONCLUSION

We have presented herein an energy-based solution method for obtaining the deflection at each point of a diaphragm. Both plate and membrane behavioral patterns can be easily derived and standardized. Therefore, in each of these two cases and with a fixed rectangularity, only one solution is needed in order to determine the deflection for every geometrical (size, thickness) and physical (applied pressure, flexural rigidity or initial internal stress) parameter. We have also presented the limit for these two cases and the solution technique for the general case using the same standardization principle. This solution method was then applied to the more complicated case of electrostatic actuation. With this actuation, we developed a standardization of the deflection as well as an abacus that allows easily identifying the deflection for both cases. Lastly, the very distinct behavioral patterns associated with the plate and membrane cases were exhibited through a study performed on a conformable electrostatic micromirror.

REFERENCES

[1] L. Landau and E. Lifshitz, *Theory of Elasticity*, Mir, Moscow, 1967

[2] R. Legtenberg, J. Gilbert, S.D. Senturia and M. Elwenspoek, Electrostatic curved electrode actuators, *IEEE Journal of Microelectromechanical Systems, vol.6, n°3 (September 1997) pp. 257-265*

[3] G. Blasquez, Y. Naciri, P. Blondel, N. Ben Moussa and P. Pons, Static response of miniature capacitive pressure sensors with square or rectangular silicon diaphragm, *Revue Phys. Appl. Vol 22 (1987), pp505-510*

[4] S. Timoshenko and S. Woinowski-Krieger. *Theory of plates and Shells*, McGraw-Hill, New York, 2nd edn, 1959

[5] E. Bonnotte, *Etude des proprietes mecaniques des films minces. Application au silicium monocristallin*, PhD Thesis, Besançon, December 1994

[6] J.I. Seeger, S.B. Crary, Analysis ans simulation of MOS capacitor feedback for stabilizing electrostatically actuated mechanical devices, Microsim II, Computational mechanics publications, pp 199-209

[7] O. Français, I. Dufour, E. Sarraute, Analytical static modeling and optimisation of electrostatic micropumps, Journal of micromechanics and microengineering, 1997, Vol 7, pp 183-185